ChemComm

COMMUNICATION

View Article Online
View Journal | View Issue

Cite this: *Chem. Commun.*, 2026, **62**, 8426

Received 3rd November 2025,
Accepted 30th March 2026

DOI: 10.1039/d5cc06240c

rsc.li/chemcomm

Triptycene-grafted helicenes: modular synthesis and key properties

Pattarakiat Seankongsuk,[a] Martin Vacek,[a] Jiří Rybáček,[a] Jaroslav Vacek,[a] Katsiaryna Kutsenka,[a] Lucie Bednárová,[a] Radek Pohl,[a] Ivana Císařová,[b] Irena G. Stará *[a] and Ivo Starý *[a]

Racemic and enantiopure ditriptyceno[*n*]helicenes (*n* = 5–7) were accessed *via* a modular, straightforward synthesis, enabling a systematic comparison of their conformational dynamics, solubility, electronic and (chir)optical properties with those of the parent helicenes.

Helicenes represent a prominent class of helically twisted polycyclic aromatic hydrocarbons[1] whose unique structural chirality and extended π-conjugation endow them with properties attractive for, *e.g.*, asymmetric catalysis,[2,3] chiroptics[4,5] and spintronics,[6–8] spin-polarised charge transport,[9–11] optoelectronics[12,13] or covalent organic frameworks.[14,15] Impressive progress in their synthesis now allows for the construction of hybrid nanographene architectures,[16] yet triptycene-grafted helicenes have gained limited attention. There are only sporadic examples of molecules where triptycene is directly annulated to a (hetero)helicene scaffold.[17,18] Also related propellane,[19] helical ladder[20] or triptycenyl helicene[21] architectures are rare. Nevertheless, triptycene, a rigid three-dimensional aromatic scaffold, continues to attract interest for imposing spatially decoupled π-systems, providing internal free volume, directing crystal packing, and suppressing deleterious aggregation.[22,23]

Herein, we report a concise synthetic route to a family of ditriptyceno[*n*]helicenes (*n* = 5–7) **1**–**3** (Fig. 1) and a comprehensive characterisation of their electronic and (chir)optical properties, barrier to racemisation, capricious solubility and crystal packing.

The preparation of racemic ditriptycenohelicenes **1**–**3** builds on our previously developed synthesis of dibenzohelicenes.[24] In this study, we first addressed a straightforward access to *o*-alkynylated triptycene boronic acid **8** (Scheme 1). In the first step, addition of the aryne generated *in situ* from 1,4-dibromo-2,5-diiodobenzene **5** to anthracene **4** (both commercially available) furnished bromoiodotriptycene **6** in yields exceeding literature reports.[25] After chemoselective alkynylation of **6** with (triisopropylsilyl)acetylene, the bromotriptycene derivative **7** was smoothly converted to the respective boronic acid **8**. Thereafter, a unified synthetic sequence delivered ditriptycenohelicenes **1**–**3** (Scheme 2). First, *o*-alkynylated triptycene boronic acid **8** was subjected to Suzuki–Miyaura cross-coupling with the homologous tolane-type dibromides **9**,[26] **12**[24] and **15**[26] to receive protected triynes **10**, **13** and **16** in high yield. Desilylation proceeded smoothly; however, only compound **11** could be routinely purified, as **14** and **17** showed poor solubility. The compound **14** became sparingly soluble after short-column chromatography and solvent evaporation, while **17** precipitated during the reaction. We nonetheless exposed all triynes to $RhCl(PPh_3)_3$-catalysed [2 + 2 + 2] cycloisomerisation in chlorobenzene under high-temperature microwave conditions. While **11**, being soluble, delivered the target ditriptyceno[5]helicene **1** in good yield, the aggregated triynes **14** and **17** afforded ditriptyceno[6]helicene **2** and ditriptyceno[7]helicene **3** in modest but acceptable yields.

The solubility of racemic ditriptycenohelicenes **1**–**3** in organic solvents deserves a brief comment. In general, grafting triptycene end-caps to termini of planar π-systems can markedly enhance solubility by suppressing π–π stacking and introducing free volume, whereas a single triptycene cap primarily

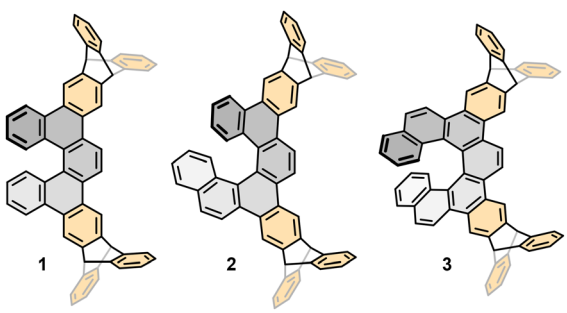

Fig. 1 Ditriptyceno[*n*]helicenes (*n* = 5–7) **1**–**3** presented in this study (only *P* enantiomers shown).

[a] *Institute of Organic Chemistry and Biochemistry, Czech Academy of Sciences, Flemingovo nám. 2, 166 10 Prague 6, Czech Republic. E-mail: stara@uochb.cas.cz, stary@uochb.cas.cz*

[b] *Department of Inorganic Chemistry, Faculty of Science, Charles University in Prague, Hlavova 2030/8, Prague 128 43, Czech Republic*

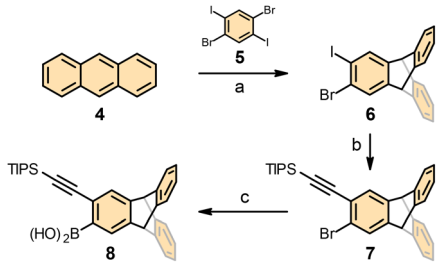

Scheme 1 Access to *o*-alkynylated triptycene boronic acid **8** as a key building block. (a) 1,4-dibromo-2,5-diiodobenzene **5** (1.7 equiv.), *n*-BuLi (1.7 equiv.), toluene, 0 °C to rt, 20 h, 41%; (b) (triisopropylsilyl)acetylene (1.7 equiv.), $Pd(PPh_3)_2Cl_2$ (3 mol%), CuI (6 mol%), toluene-diisopropylamine (1 : 1), 35 °C, 1 h, 70%; (c) *n*-BuLi (1.6 equiv.), THF, −78 °C, 30 min, then triisopropyl borate (2.4 equiv.), −78 °C to rt, 2 h, then HCl (2 M, aq.), rt, 1 h, 85%.

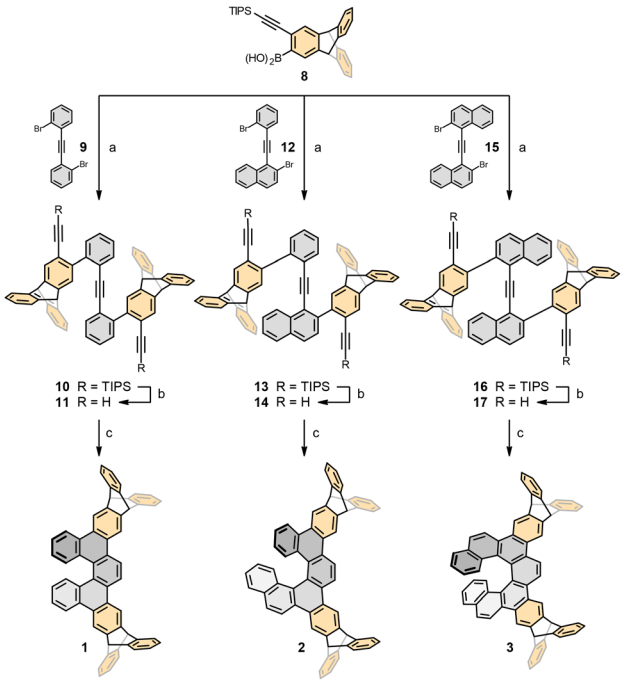

Scheme 2 Synthesis of ditriptycenohelicenes **1**–**3** (only *P* enantiomers shown). (a) *o*-alkynylated triptycene boronic acid **8** (2.3–2.4 equiv.), $Pd(PPh_3)_2Cl_2$ (5 mol%), Cs_2CO_3 (3.2–3.3 equiv.), toluene-ethanol-water (4.3 : 4.3 : 1), 90 °C, 1.5–3 h, **10** : 83%, **13** : 90%, **16** : 84%; (b) TBAF in THF (1 M, 2.2–2.3 equiv.), THF-methanol (100 : 1), 0 °C to rt, 1 h, **11** : 79% or THF, −10 °C to 0 °C, 1 h, crude **14** and **17** were used directly in the following step due to poor solubility; (c) Wilkinson's catalyst (10–15 mol%), chlorobenzene, microwave reactor, 160 °C, 20–30 min, **1** : 71%, **2** : 48%, **3** : 27%.

modulates solid-state packing.[25,27] For instance, a large improvement of solubility in organic solvents by the factor of 70 was described for indigo pigments.[28] Unexpectedly, ditriptycenohelicene **1** and, in particular, the higher homologues **2** and **3** exhibited markedly reduced solubility relative to the parent helicenes **18**–**20**. An exception was **2** in toluene, where the "triptycene effect" afforded increased solubility (Table 1).

The single-crystal XRD analysis of the racemic ditriptycenohelicene **3** rationalises its reduced solubility (Fig. 2). The compound crystallises as a racemic mixture with two *M*/*P* pairs per unit cell. Homochiral molecules assemble into columns along the A axis, interlaced with disordered THF. While the multiple C–H···π contacts produce a dense, interdigitated lattice, the parallel-displaced π–π interactions are not present in the crystal.

Table 1 Solubility of racemic ditriptycenohelicenes **1**–**3** *vs.* parent [5]-, [6]- and [7]helicene **18**–**20**

Helicene	Solubility in CH_2Cl_2 (mg ml^{-1})[a]	Solubility in toluene (mg ml^{-1})[a]
1	>50	>50
[5]Helicene **18**	>80	>80
2	32	230
[6]Helicene **19**	66	28
3	31	11
[7]Helicene **20**	67	18

[a] Determined at 22 °C, values are within an estimated error of ±10%.

Racemic ditriptycenohelicenes **1**–**3** were resolved into enantiomers by chiral HPLC on analytical (**1**) and also semipreparative (**2** and **3**) scale (*rac*-**1**: Chiralpak IC (DAICEL), *rac*-**2** and *rac*-**3**: ChiralArt Cellulose-SA (YMC)) to enable studies of configurational dynamics and chiroptical properties. The experimental barriers to racemisation, determined by dynamic chiral HPLC[29] (**1**) or by monitoring reversible first-order racemisation kinetics (**2**), agree reasonably with the calculated values and are quite close to those of the parent [5]-, [6]- and [7]helicene **18**–**20** (Table S4).

Gas-phase DFT B3LYP-D3/cc-pVTZ calculations show that the frontier orbitals (HOMO/LUMO) of **1**–**3** are localised almost entirely on the central part of the native helicene scaffold, whereas the adjacent levels (HOMO−1/LUMO+1) extend onto the triptycene blades fused to the helix, as illustrated for ditriptyceno[7]helicene **3** (Fig. 3). Calculated HOMO–LUMO gaps (related to the first excited singlet state) and the optical HOMO–LUMO gaps (calculated from absorption spectra) fall in a narrow range of *ca* 3.50–3.72 eV and decrease slightly from **1**

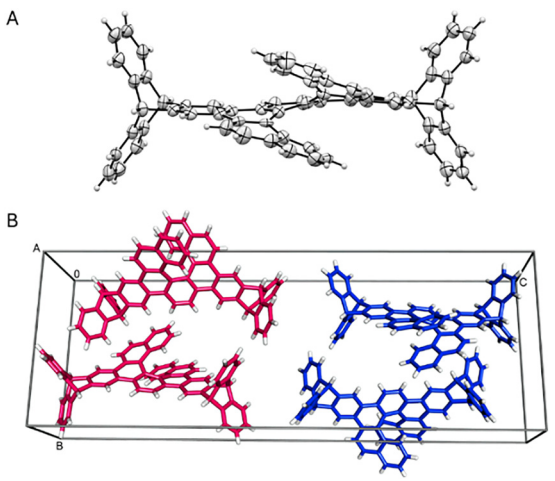

Fig. 2 Views of the single-crystal XRD structure of the racemic ditriptyceno[7]helicene **3**: (A) molecular structure and (B) crystal packing (CCDC 2492687). ORTEP thermal ellipsoids are drawn at the 50% probability level. The *M* (red) and *P* (blue) enantiomers in the unit cell are shown as stick models; disordered co-crystallised THF is omitted.

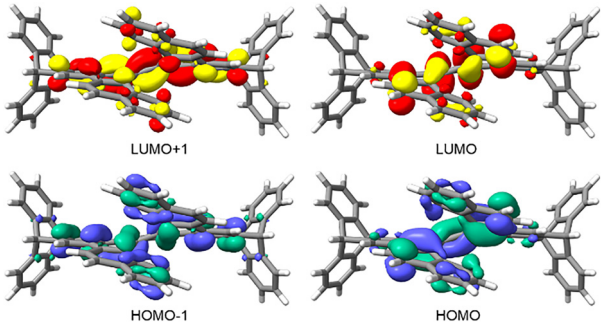

Fig. 3 The frontier molecular orbitals of the ditriptyceno[7]helicene **3** calculated by DFT B3LYP/cc-pVTZ/GD3. Grey: carbon, white: hydrogen, orbital isovalue ±0.03 a.u.

to **3** as the π-conjugated framework extends (Table S2). The electronic behaviour of ditriptycenohelicenes **1**–**3** follows that of the parent [5]-, [6]- and [7]helicene **18**–**20**.

The UV–Vis spectra of ditriptycenohelicenes **1**–**3** show the characteristic multiband profile of π-extended systems, with intense bands across 250–360 nm. The absorption onset shifts modestly to longer wavelength with increasing helical length (≈400 nm for **1**, 410 nm for **2** and 420 nm for **3**), indicating progressive π-conjugation and a gradual narrowing of the HOMO–LUMO gap (Fig. 4, Table S2). The fluorescence spectra are devoid of multiband character or pronounced vibronic structure, except for the hexahelicene derivative **2**, which displays a faint shoulder. The emission maxima follow a similar bathochromic trend, shifting from 431 nm for **1** and 432 nm for **2** to 446 nm for **3**.

Electronic circular dichroism (ECD) spectra of enantiopure **2** and **3** display clean, near-ideal mirror-image profiles for each enantiomeric pair (Fig. 5 and Fig. S23–S24). The longest- wavelength Cotton effect is positive for the *P* enantiomers and negative for the *M* enantiomers (*ca.* 330–380 nm for **2** and 340–410 for **3**), in line with the empirical helicene sign rule and our TD-DFT simulations (see SI). The overall spectral intensity is markedly diminished compared to the parent helicenes, consistent with observations made for the

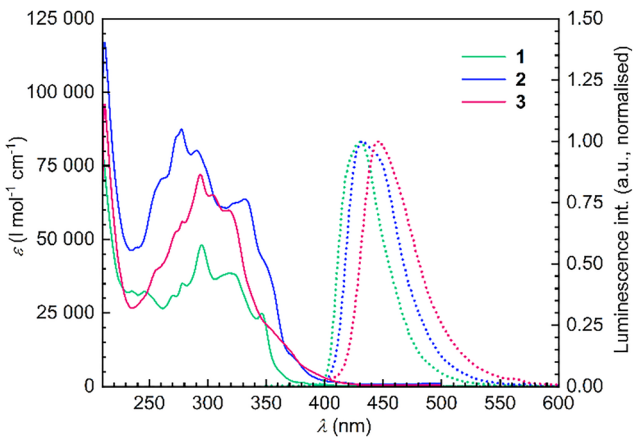

Fig. 4 UV-Vis (full lines, 10^{-4} M in THF) and fluorescence spectra (dotted lines, 10^{-5} M in THF, exc. 345 nm for **1**, 286 nm for **2**, 282 nm for **3**) of ditriptyceno-helicenes **1**–**3**.

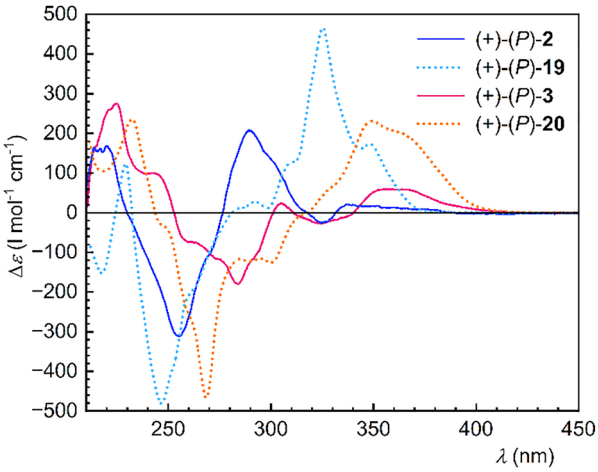

Fig. 5 ECD spectra of ditriptycenohelicenes **2** and **3** (full lines) and parent helicenes **19** and **20** (dotted lines) (10^{-4} M in THF).

dibenzohelicene series.[24] The absolute configurations (−)-*M* and (+)-*P* were unambiguously assigned to the isolated enantiomers of **2** and **3** based on comparison of their ECD spectra with those of the reference parent helicenes **19** and **20** and the computed ones.

In comparison to the parent helicenes **19** and **20**, the chiroptical responses of the ditriptycenohelicenes **2** and **3** are attenuated, as evidenced by their smaller $|\Delta\varepsilon|$ values in the ECD spectra (*vide supra*) and markedly reduced specific rotations $[\alpha]_D^{20}$: −155/+162 for (−)-(*M*)/(+)-(*P*)-**2** (chloroform) *vs.* −3 629/+3 676 for (−)-(*M*)/(+)-(*P*)-**19** (dichloromethane)[30] or -415/+ 420 for (−)-(*M*)/(+)-(*P*)-**3** (chloroform) *vs.* −5 164/+5 101 for (−)-(*M*)/(+)-(*P*)-**20** (dichloromethane).[30] On the other hand, the modest values of the luminescence dissymmetry factor $|g_{lum}|$ obtained from the CPL spectra are comparable across the two classes of helicenes: 2.3×10^{-3} (425 nm, THF) for **2** *vs.* 0.9×10^{-3} (*ca* 424 nm, dichloromethane) for **19**[31] and 0.9×10^{-3} (430 nm, THF) for **3** *vs.* 6×10^{-3} (450 nm, chloroform) for **20**.[32]

Similarly to the parent [6]helicene **19**, the g_{lum} value for the ditriptyceno[6]helicene (+)-(*P*)-**2** is negative. In contrast, the situation differs for ditriptyceno[7]helicene (+)-(*P*)-**3** compared to the parent [7]helicene (+)-(*P*)-**20**. Whereas the latter reference compound exhibits a positive g_{lum} factor, (+)-(*P*)-**3** displays a bisignate CPL spectrum, with a more intense blue-shifted negative band in THF and a red-shifted positive band that predominates in toluene (Fig. 6A). To clarify the behaviour of (+)-(*P*)-**3**, we calculated its excited-state properties and CPL luminescence dissymmetry factors for the lowest-energy states, S_1 ("bright") and S_2 ("dark"), both possessing predominantly a π → π* character (Table S5). In addition, we recorded temperature-dependent CPL spectra of (+)-(*P*)-**3** (Fig. S30) and measured its fluorescence lifetime, including that of **1** and **2** (Table S6). To explain the bisignate character of the CPL spectrum of (+)-(*P*)-**3**, we propose the coexistence of two distinct emissive pathways: (i) The $S_1 \rightarrow S_0$ transition, observed and calculated at *ca* 490 nm, involves an S_1 state that is structurally compressed, with the terminal helicene rings separated by approximately 3.5 Å (*cf.* 4.0 Å in S_0), thereby promoting a

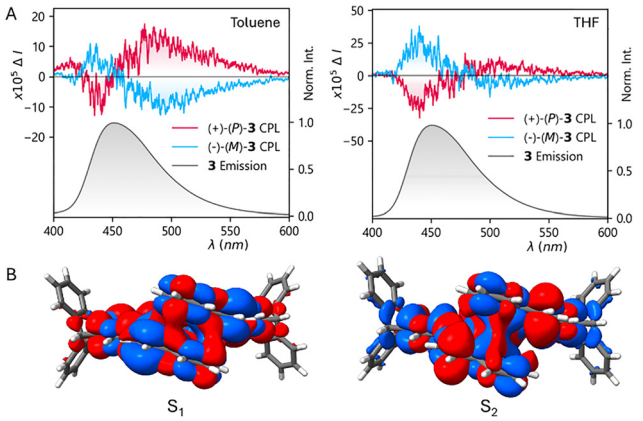

Fig. 6 (A) CPL spectra of ditriptyceno[7]helicene (+)-(*P*)- and (−)-(*M*)-**3** in toluene and THF, 10^{-5} M; (B) localisation of the NTOs for the S_1 and S_2 excited states of (−)-(*M*)-**3** (blue: hole orbital, red: particle orbital, orbital isovalue ±0.01 a.u.; CAM-B3LYP/cc-pVTZ/GD3).

transannular vibronic coupling (Fig. 6B, S31). (ii) The $S_2 \rightarrow S_0$ transition, observed at *ca* 430 nm (calcd. at *ca* 390 nm), involves an S_2 state that is structurally more relaxed, with the terminal helicene rings separated by approximately 4.3 Å. Then, non-adiabatic S_1–S_2 coupling renders a "dark" S_2 state partially bright because, during internal conversion, vibronic mixing (activated by a low-frequency "breathing" mode of the helicene scaffold in the range of 28–40 cm^{-1}) enables it to borrow part of the electric dipole intensity from a nearby bright S_1 state (*cf.* Herzberg–Teller intensity borrowing).[33] It is worth noting that the S1/S2 PES crossing occurs along the "breathing" mode coordinate. This vibronic coupling is further modulated by the solvent environment and temperature, lending additional support to this model (for a discussion, see Fig. S32).

In summary, we have prepared a series of racemic and enantiopure ditriptyceno[*n*]helicenes (*n* = 5–7) **1**–**3**, a hybrid family hitherto unreported in the literature. Grafting two triptycene units onto the helicene scaffolds does not substantially perturb their conformational dynamics and electronic or optical properties relative to the parent helicenes. However, the ditriptycenohelicenes show some differences such as slightly reduced optical HOMO–LUMO gaps, mostly attenuated chiroptical responses and incoherent solubility.

P. Seankongsuk synthesised and characterised triptycene-grafted helicenes **2** and **3**, carried out solubility tests and contributed to the SI. M. Vacek pioneered the synthesis and characterisation of triptycene-grafted helicene **1**, calculated its racemisation barrier and contributed to the SI. J. Rybáček performed DFT calculations, supervised chiral separations, interpreted the ECD spectra, contributed to the SI and co-wrote the manuscript. J. Vacek carried out DFT calculations, interpreted the CPL spectra and co-wrote the manuscript. K. Kutsenka supervised the synthesis and characterisation of triptycene-grafted helicene **1**, measured and interpreted fluorescence lifetimes. L. Bednárová measured and interpreted the (chir)optical spectra. R. Pohl recorded and interpreted the NMR spectra. I. Císařová conducted the single-crystal XRD analysis. I. G. Stará and Ivo Starý conceived and directed the project and co-wrote the manuscript. All authors contributed to the writing and verified the experimental data.

Conflicts of interest

There are no conflicts to declare.

Data availability

The data that support this article have been included in the supplementary information (SI). supplementary information: synthesis and characterisation data of new compounds including HPLC resolution of enantiomers, (chir)optical spectra, racemisation barriers and computational details. See DOI: https://doi.org/10.1039/d5cc06240c.

CCDC 2492687 contains the supplementary crystallographic data for this paper.[34]

Acknowledgements

We are grateful to the Czech Science Foundation (Reg. No. 24-10787S) and the Institute of Organic Chemistry and Biochemistry, Czech Academy of Sciences (RVO: 61388963) for their funding of this research. I.S. gratefully acknowledges the support of the Praemium Academiae of the Czech Academy of Sciences. We thank IOCB Core Facilities for technical assistance in the characterisation of the compounds.

References

1 *Helicenes: Synthesis, Properties and Applications*, ed. J. Crassous, I. G. Stará and I. Starý, John Wiley & Sons, Ltd, Weinheim, 2022.
2 D. Sakamoto, I. Gay Sánchez, J. Rybáček, J. Vacek, L. Bednárová, M. Pazderková, R. Pohl, I. Císařová, I. G. Stará and I. Starý, *ACS Catal.*, 2022, **12**, 10793–10800.
3 T. Edlová, J. Rybáček, H. Cattey, J. Vacek, L. Bednárová, P. Le Gendre, A. T. Normand, I. G. Stará and I. Starý, *Angew. Chem., Int. Ed.*, 2025, **64**, e202414698.
4 J. Crassous, M. J. Fuchter, D. E. Freedman, N. A. Kotov, J. Moon, M. C. Beard and S. Feldmann, *Nat. Rev. Mater.*, 2023, 365–371.
5 I. Shioukhi, H. Batchu, G. Schwartz, L. Minion, Y. Deree, B. Bogoslavsky, L. J. W. Shimon, J. Wade, R. Hoffman, M. J. Fuchter, G. Markovich and O. Gidron, *Angew. Chem., Int. Ed.*, 2024, **63**, e202319318.
6 A. Borissov, P. J. Chmielewski, C. J. Gómez García, T. Lis and M. Stępień, *Angew. Chem., Int. Ed.*, 2023, **62**, e202309238.
7 S. Cadeddu, R. Chowdhury, C. Delpiano Cordeiro, S. Parmar, A. Kramer, M. Cordier, A. Pensel, N. Vanthuyne, R. Sessoli, M. Chiesa, Y.-K. Liao, R. H. Friend, E. Salvadori, J. Autschbach and J. Crassous, *J. Am. Chem. Soc.*, 2025, **147**, 23643–23653.
8 J. Borstelmann, S. Zank, M. Krug, G. Berger, N. Fröhlich, G. Glotz, F. Gnannt, L. Schneider, F. Rominger, F. Deschler, T. Clark, G. Gescheidt, D. M. Guldi and M. Kivala, *Angew. Chem., Int. Ed.*, 2025, **64**, e202423516.
9 V. Kiran, S. P. Mathew, S. R. Cohen, I. Hernández Delgado, J. Lacour and R. Naaman, *Adv. Mater.*, 2016, **28**, 1957–1962.
10 R. Rodríguez, C. Naranjo, A. Kumar, P. Matozzo, T. K. Das, Q. Zhu, N. Vanthuyne, R. Gómez, R. Naaman, L. Sánchez and J. Crassous, *J. Am. Chem. Soc.*, 2022, **144**, 7709–7719.
11 M. R. Safari, F. Matthes, C. M. Schneider, K.-H. Ernst and D. E. Bürgler, *Small*, 2024, **20**, 2308233.
12 Y. Yang, R. C. da Costa, M. J. Fuchter and A. J. Campbell, *Nat. Photonics*, 2013, **7**, 634–638.
13 W.-C. Guo, W.-L. Zhao, K.-K. Tan, M. Li and C.-F. Chen, *Angew. Chem., Int. Ed.*, 2024, **63**, e202401835.
14 Q. Yan, S. Tao, R. Liu, Y. Zhi and D. Jiang, *Angew. Chem., Int. Ed.*, 2024, **63**, e202316092.

15 J. del, R. Monroy, T. Deshpande, J. Schlecht, C. Douglas, R. Stirling, N. Grabicki, G. J. Smales, Z. Kochovski, F. G. Fabozzi, S. Hecht, S. Feldmann and O. Dumele, *J. Am. Chem. Soc.*, 2025, **147**, 17750–17763.
16 N. Martin and C. P. Nuckolls, *Molecular Nanographenes: Synthesis, Properties, and Applications*, John Wiley & Sons, 2025.
17 H. Mubarok, A. Amin, T. Lee, J. Jung, J.-H. Lee and M. H. Lee, *Angew. Chem., Int. Ed.*, 2023, **62**, e202306879.
18 K.-K. Tan, M. Li and C.-F. Chen, *Chem. Commun.*, 2025, **61**, 11191–11194.
19 J. Ma, X. Liu, F. Hao and L. Zhang, *Angew. Chem., Int. Ed.*, 2025, **64**, e202503225.
20 T. Ikai, T. Yoshida, K. Shinohara, T. Taniguchi, Y. Wada and T. M. Swager, *J. Am. Chem. Soc.*, 2019, **141**, 4696–4703.
21 T. R. Kelly, *Acc. Chem. Res.*, 2001, **34**, 514–522.
22 M. N. Khan and T. Wirth, *Chem. – Eur. J.*, 2021, **27**, 7059–7068.
23 F. Ishiwari, Y. Shoji, C. J. Martin and T. Fukushima, *Polym. J.*, 2024, **56**, 791–818.
24 A. Jančařík, J. Rybáček, K. Cocq, J. Vacek Chocholoušová, J. Vacek, R. Pohl, L. Bednárová, P. Fiedler, I. Císařová, I. G. Stará and I. Starý, *Angew. Chem., Int. Ed.*, 2013, **52**, 9970–9975.
25 L. Ueberricke, J. Schwarz, F. Ghalami, M. Matthiesen, F. Rominger, S. M. Elbert, J. Zaumseil, M. Elstner and M. Mastalerz, *Chem. – Eur. J.*, 2020, **26**, 12596–12605.
26 H.-K. Chang, S. Datta, A. Das, A. Odedra and R.-S. Liu, *Angew. Chem., Int. Ed.*, 2007, **25**, 4744–4747.
27 L. Ueberricke and M. Mastalerz, *Chem. Rec.*, 2021, **21**, 558–573.
28 B. P. Benke, L. Hertwig, X. Yang, F. Rominger and M. Mastalerz, *Eur. J. Org. Chem.*, 2021, 72–76.
29 O. Trapp, *J. Chromatogr. B*, 2008, **875**, 42–47.
30 M. Šámal, J. Rybáček, J. Holec, J. Hanus, J. Vacek, M. Buděšínský, L. Bednárová, P. Fiedler, M. Š. Slušná, I. G. Stará and I. Starý, *Chem. Commun.*, 2022, **58**, 12732–12735.
31 H. Tanaka, M. Ikenosako, Y. Kato, M. Fujiki, Y. Inoue and T. Mori, *Commun. Chem.*, 2018, **1**, 1–8.
32 H. Kubo, T. Hirose, T. Nakashima, T. Kawai, J. Hasegawa and K. Matsuda, *J. Phys. Chem. Lett.*, 2021, **12**, 686–695.
33 Y. Liu, J. Cerezo, G. Mazzeo, N. Lin, X. Zhao, G. Longhi, S. Abbate and F. Santoro, *J. Chem. Theory Comput.*, 2016, **12**, 2799–2819.
34 CCDC 2492687: Experimental Crystal Structure Determination, 2026, DOI: 10.5517/ccdc.csd.cc2pnv8h.

